

**SYNTHESIS AND OPTIMIZATION OF COPPER OXIDE AS P-TYPE
TRANSPARENT CONDUCTING OXIDE**

By

NUR AIMI JANI

**Dissertation submitted in fulfillment of the
requirements for the degree
of Master of Science**

May 2010

ACKNOWLEDGEMENT

First and foremost, I would like to express my gratefulness to Allah SWT for the completion of this dissertation. My heartiest and deepest gratitude to my supervisor, Dr. Zainovia Lockman whose encouragement, guidance and continuous support from the initial to the final level enable me to develop an understanding of the project. I wish to express my sincere thanks to my co- supervisor Prof. Ahmad Fauzi Mohd Noor. His wide knowledge and logical thinking have been a great value for me in completing this work.

A special gratitude to my lovely husband and daughter for their love, and also to my beloved family members especially my parents-in-law, Hjh. Nurul Huda and Hj. Hamdan for their undying support, their faith in me and for taking care of me and my daughter during my stay with them and also not forgetting my mother and father, Pn. Rosina Binti Mohamed and En. Jani Bin Kasbullah and my dearest siblings for their undying love that they have shown to me all along. I love you all. Thank you very much.

I would also like to express my sincere appreciation to other lecturers, technicians and staffs in School of Materials and Mineral Resources Engineering for helping me by giving their suggestions and cooperation in making this study a success.

Lastly, I also like to thank all of those who supported me in any respect during the completion of the project especially to Universiti Sains Malaysia (USM), for giving me a fellowship for me to study and also to all my fellow friends. Thank you very much.

TABLE OF CONTENTS

	Page
ACKNOWLEDGEMENT	ii
TABLE OF CONTENTS	iii
LIST OF TABLES	vii
LIST OF FIGURES	ix
LIST OF ABBREVIATIONS	xiv
LIST OF SYMBOLS	xvi
ABSTRAK (BAHASA MELAYU)	xvii
ABSTRACT	xviii
CHAPTER 1 : INTRODUCTION	
1.1 Introduction	1
1.2 Problem Statement	3
1.3 Objectives	4
1.4 Expected Outcomes	4
CHAPTER 2 : LITERATURE REVIEW	
2.1 Introduction	5
2.2 Transparent Conducting Oxides (TCO) Thin Film	5
2.3 Thin Films	7
2.3.1 Advantages compared with traditional bulk materials	7
2.3.2 Thin film growth mode	8
2.4 Different Types of TCO Materials	9
2.4.1 n-type TCO	11
2.4.2 p-type TCO	12
2.4.2.1 Origin of conductivity of p-type TCO	13

2.4.2.2	Delafossite Crystal Structure	15
2.5	Applications of TCO Thin Film	17
2.5.1	Flat Panel Display	18
2.5.2	Functional Window	18
2.6	Copper Oxide Thin Film	18
2.6.1	Cuprous Oxide (Cu ₂ O)	19
2.6.2	Cupric Oxide (CuO)	19
2.7	Deposition Techniques for Thin Copper Oxide Films	20
2.7.1	Sputtering	22
2.7.2	Thermal Oxidation	23
2.7.3	Electrodeposition	24
2.7.4	Chemical Solution Deposition (CSD) Methods	25
2.7.4.1	Requirements in CSD Technique	26
2.7.4.2	Precursor Solution Processes and Chemical Routes	27
(a)	Sol-gel route	28
(b)	Metal-organic decomposition (MOD) process	28
(c)	Nitrate route	29
2.8	Coating Techniques	29
2.8.1	Spin-coating	30
2.8.2	Spray-coating	30
2.8.3	Dip-coating	31
2.8.3.1	The optical and electrical properties of the thin CuO films prepared by CSD techniques	33
2.9	All Transparent Conducting Oxide (TCO) p-n Junction	36
 CHAPTER 3 : METHODOLOGY		
3.1	Introduction	42

3.2	Experiment 1: Technique for the formation of thin copper oxide film	44
3.3	Procedure of Experiment	44
3.3	Raw Materials	46
3.3.1	Copper Source: Copper (II) Nitrate ($\text{Cu}(\text{NO}_3)_2 \cdot 2\frac{1}{2}\text{H}_2\text{O}$)	46
3.3.2	Solvent: Methanol(CH_3OH)	46
3.3.3	Solvent: Ethanol	47
3.3.4	Wetting Agent: Ethanolamine, EA ($\text{NH}_2\text{CH}_2\text{CH}_2\text{OH}$)	47
3.4	Preparation of precursor solution	48
3.5	Preparation of substrate	49
3.6	Deposition and drying process	50
3.6.1	Annealing processes	51
3.8	Summary of the formation of thin copper oxide film	45
3.7	Experiment Parameters	52
3.7.1	Sample preparation	55
3.7.2	Effect of the concentration copper nitrate ($\text{Cu}(\text{NO}_3)_2 \cdot 2\frac{1}{2}\text{H}_2\text{O}$)	57
3.7.3	Effect of the number of coatings	57
3.7.4	Effect of the withdrawal rate	57
3.7.5	Effect of the annealing temperature and time	58
3.8	Experiment 2: Formation of p-n Junction TCOs	59
3.9	Characterization Techniques	59
3.9.1	Field Emission Scanning Electron Microscopy	60
3.9.2	X-ray diffraction spectrometry (XRD)	61
3.9.3	Ultra-violet visible spectrometry (UV-Vis)	62
3.9.4	Atomic Force Microscopy (AFM)	63
3.9.5	Two-point Probe System (Sheet Resistance Analysis)	64
3.9.5.1	Sheet Resistance	65

3.9.5.2	Resistance and conductivity measurements	65
---------	--	----

CHAPTER 4 : RESULTS AND DISCUSSION

4.1	Introduction	67
4.2	Formation of Thin Copper Oxide Film by Dip Coating	67
4.2.1	The Effect of Concentration of Copper Nitrate ($\text{Cu}(\text{NO}_3)_2 \cdot 2\frac{1}{2}\text{H}_2\text{O}$)	76
4.2.2	The Effect of Number of Coatings	97
4.2.3	The Effect of Withdrawal Rate	115
4.2.4	The Effect of Substrates and Surfactants	128
4.2.5	The Effect of Annealing on The Formation of CuO and Cu ₂ O in Air and Ar-H ₂ Gas	131
4.3	The Formation of Transparent Semiconductor p-n Junction	140

CHAPTER 5 : CONCLUSION AND SUGGESTION

5.1	Conclusion	146
5.2	Suggestions and Recommendations	148

REFERENCES	149
-------------------	-----

APPENDICES	158
-------------------	-----

LIST OF PUBLICATIONS	166
-----------------------------	-----

LIST OF TABLES

Table 2.1	Crystal structure of most commonly studied p- and n-type TCOs [Barsoum et al., 2003; Yanagi et al., 2000; Ingram et al., 2004; Norton et al., 2004]	10
Table 2.2	The electrical properties of different n-type TCO [Jia et al., 2003]	12
Table 2.3	The electrical properties of different p-type TCO [Jia et al., 2003; Nair et al., 1999; Kose et al., 2008]	17
Table 2.4	Physical Properties of Cu ₂ O and CuO	20
Table 2.5	List of the research work on thin p-type TCO films based on CuO using different technique of deposition	21
Table 2.6	Summary of literature on the formation of thin CuO and Cu ₂ O thin film by CSD at different annealing temperature	36
Table 3.1	Physical properties of the typical solvent [Brinker at al., 1990]	47
Table 3.2	Summary of samples at different parameters for thin CuO film formation by CSD technique	53
Table 3.3	List of the number of sample preparation and characterization	55
Table 3.4	Parameters that were kept constant used for the formation of deposition solution at different concentration of Cu (NO ₃) ₂ .2 ¹ / ₂ H ₂ O.	56
Table 3.5	Parameters that were kept constants for effect of number of coatings	57
Table 3.6	Parameters that were kept constants for effect of withdrawal rate	58
Table 4.1	The characteristics of chemical bonding for each compound present in the as-deposited films from FTIR analysis	74
Table 4.2	Observations of the physical properties of the coating after deposition and after heat treatment as a function of the concentration of Cu (NO ₃) ₂ .	77
Table 4.3	Mechanism of film formation as a function of three levels of concentration: low concentration, intermediate	88

concentration and high concentration.

Table 4.4	The RMS roughness values evaluated by AFM for different concentrations of Cu (NO ₃) ₂ from 90 to 300 mmol.	88
Table 4.5	Electrical conductivities of thin CuO films as a function of concentrations	97
Table 4.6	Observations of the general appearance of the coatings after deposition and after heat treatment as a function of the number of coatings.	98
Table 4.7	The electrical conductivities of CuO films with (a) 3, (b) 5, and (c) 7 coatings	114
Table 4.8	Summary of the appearance of the coatings made at different withdrawal rates after deposition and after heat treatment.	116
Table 4.9	The electrical conductivities of CuO films at different withdrawal rates, (a) 0.1, (b) 1.0, (c) 2.0 and (d) 3.0 cm/min	127
Table 4.10	Observations of the general appearance of the coatings after deposition and after heat treatment on different types of substrates.	129
Table 4.11	Summary of the FWHM and the crystallite size of CuO film after being heated from 250 °C to 500 °C in air and Ar-H ₂ gas.	134
Table 4.12	The electrical conductivities of CuO films at different annealing temperatures: (a) 250, (b) 300, (c) 350, (d) 400 and (e) 500 °C	140

LIST OF FIGURES

Figure 1.1	A schematic illustration of the transparent p-n junction conducting oxides films	3
Figure 2.1	Schematic illustrating the band gap designing for TCO [Chattopadhyay et al., 2005]	6
Figure 2.2	Common modes of film growth; (a) Island (volmer - Weber) mode, (b) layer-by-layer (Frank-Van der merwe) mode and (c) Mixed (Stranski-krastanov) mode	9
Figure 2.3	Schematic diagram of modulation of band structure (CMVB) Cations are assumed to have a closed shell the energy of which is equivalent to that of O 2p ⁶ [Chattopadhyay et al., 2005]	14
Figure 2.4	Crystal structure of delafossite consisting of stacked layers of -O-Ga(Al)-O-Cu-O- in this order along the c-axis [Yanagi et al., 2000]	16
Figure 2.5	Flow chart of a typical chemical solution deposition (CSD) process	26
Figure 2.6	Illustration of commonly used coating techniques [Schwarz et al., 2004]	29
Figure 2.7	Three stages for dip coating process (a) immersion, (b) withdrawal and (c) deposition [Brinker et al., 1990]	32
Figure 2.8	Schematic diagram of the steady state deposition stage of the dip coating process [Brinker et al., 1990]	33
Figure 2.9	The schematic diagram of the (a) transparent hetero-junction diode of the form: glass/ITO/p-SrCu ₂ O ₂ /n-ZnO/n ⁺ -ZnO and (b) rectifying I-V characteristics of p-n hetero-junction [Sato et al., 1993]	37
Figure 2.10	The schematic diagram of the (a) diode structure and (b) I-V characteristic [Chiu et al. 2009]	38
Figure 2.11	The schematic diagram of the (a) diode structure and (b) transmittance spectra [Chattopadhyay et al. 2007]	39
Figure 2.12	The schematic diagram of the diode structure and I-V characteristic [Liu et al. 2004]	40
Figure 2.13	The schematic diagram of the (a) diode structure and (b) transmittance spectra [Tonooka et al. 2003]	40

Figure 2.14	The schematic diagram of the (a) diode structure and (b) the I-V characteristic [Yanagi et al. 2002]	41
Figure 3.1	Flow chart of the experiments conducted	43
Figure 3.2	The schematic diagram of the p-n junction system	43
Figure 3.3	The flow chart of chemical solution deposition (CSD) process	45
Figure 3.4	The schematic diagram for the formation of thin film by CSD process	46
Figure 3.5	Arrangement of substrate and coating solution during dip coating process (Alpha Dynamic Engineering Dip Coater)	50
Figure 3.6	The schematic diagram of the heat treatment process with heating and cooling rate	51
Figure 3.7	Photograph of $\text{Cu}(\text{NO}_3)_2$ dissolved with used different type of solvents (a) Methanol and (b) Ethanol	56
Figure 3.8	The overall setup of the Agilent 4165C SPA machine	66
Figure 4.1	Schematic diagram shows possible forces acting (shown by dotted arrows) on film deposited on the substrate which is withdrawn from the coating solution	70
Figure 4.2	Photograph showing the precursor solution containing 120 mmol of copper nitrate dissolved in 100 ml methanol (a) before addition of 1 ml EA, (b) after addition of 1 ml EA	72
Figure 4.3	FTIR spectra of as-deposited and as-annealed films deposited on glass substrate	73
Figure 4.4	FTIR spectra of annealed films	73
Figure 4.5	TG and DTA curve of as-deposited films	75
Figure 4.6	XRD patterns of samples prepared with different concentrations of $\text{Cu}(\text{NO}_3)_2$, after being annealed in air at 500 °C, (a) 30 mmol, (b) 60 mmol, (c) 90 mmol, (d) 120 mmol, (e) 180 mmol, (f) 240 mmol and (g) 300 mmol	79
Figure 4.7	FESEM images of samples made using different concentrations of $\text{Cu}(\text{NO}_3)_2$ (a) 30 mmol, (b) 60 mmol, (c) 90 mmol, (d) 120 mmol, (e) 180 mmol, (f) 240 mmol, (g) 300 mmol	81
Figure 4.8	FESEM images of the cross sectional view of thin CuO films prepared using different concentrations of $\text{Cu}(\text{NO}_3)_2$ (a) 60 mmol, (b) 90 mmol, (c) 120 mmol, and (d) 240	85

mmol

Figure 4.9	The schematic diagram of the mechanism of film formation at three coatings of different concentrations (a) low concentration (30 to 90 mmol), (b) intermediate concentration (120 to 180 mmol), and (c) high concentration (240 and 300 mmol)	89
Figure 4.10	AFM topography images of thin CuO films formed with different concentrations of Cu(NO ₃) ₂ (a) 90, (b) 120, (c) 180, (d) 240, and (e) 300 mmol	91
Figure 4.11	The plotted graph of RMS roughness of the films versus the concentration of Cu(NO ₃) ₂	92
Figure 4.12	The optical transmittance spectra of the CuO films formed at different concentrations of Cu (NO ₃) ₂ , (a) 30 mmol, (b) 60 mmol, (c) 90 mmol, (d) 120 mmol, (e) 180 mmol, (f) 240 mmol and (g) 300 mmol	93
Figure 4.13	The plots of $(\alpha h\nu)^2$ versus $h\nu$ as a function of solution concentration of Cu (NO ₃) ₂ represents (a) 90 mmol, (b) 120 mmol, and (c) 180 mmol	94
Figure 4.14	I-V characteristics of CuO films as a function of concentrations (a) 90 mmol, (b) 120 mmol, and (c) 240 mmol	96
Figure 4.15	XRD diffraction patterns of coatings formed on the glass substrate. The samples were coated with (a) 1, (b) 3, (c) 5, (d) 7, and (e) 10 times of coating.	100
Figure 4.16	FESEM images showing the surface morphology of different coatings on the glass substrate. Number of coatings used: (a) 1, (b) 3, (c) 5, (d) 7, and (e) 10 times of coating.	101
Figure 4.17	FESEM images showing the cross sectional view of thin CuO film prepared with (a) 3, (b) 5 and (c) 7 coatings.	104
Figure 4.18	The plotted graph of the thickness of the coating as a function of number of coatings	106
Figure 4.19	The EDX results of two samples prepared with (a) 1 coating and (b) 10 coatings	107
Figure 4.20	Schematic diagram of film formation as a function of the number of coatings	109
Figure 4.21	AFM images of thin CuO films with (a) 1, (b) 3, (c) 5 and (d) 7 coatings	110

Figure 4.22	The plotted graph of RMS of the films as a function of number of coatings	111
Figure 4.23	The optical transmittance spectra of CuO films with (a) 1, (b) 3, (c) 5, (d) 7, and (e) 10 coatings.	112
Figure 4.24	The plots of $(\alpha h\nu)^2$ versus $h\nu$ at (a) 3, and (b) 5 coatings.	113
Figure 4.25	I-V characteristic of thin CuO films with (a) 3, (b) 5, and (c) 7 coatings	114
Figure 4.26	XRD patterns of 4 samples prepared at different withdrawal rates, (a) 0.1(2 cm/min), (b) 1.0 (10 cm/min), (c)2.0 (15 cm/min), and (d) 3.0 (20 cm/min)	117
Figure 4.27	The FESEM images for samples made at different withdrawal rate (a) 0.1(2 cm/min), (b) 1.0 (10 cm/min), (c) 2.0 (15 cm/min), and (d) 3.0 (20 cm/min)	119
Figure 4.28	The schematic diagram of the coating structure deposited on the substrate with comparison of withdrawal rate at (a) 0.1(2 cm/min) and (b) 2.0 (15 cm/min)	121
Figure 4.29	The FESEM cross-sectional images of samples made at different withdrawal rates (a) 0.1(2 cm/min), (b) 1.0 (10 cm/min), (c) 2.0 (15 cm/min), and (d) 3.0 (20 cm/min)	122
Figure 4.30	AFM images of the 4 samples prepared at different withdrawal rates (a) 0.1, (b) 1.0, (c) 2.0 and (d) 3.0 cm/min	124
Figure 4.31	The plotted graph of RMS of the films as a function of withdrawal rate	125
Figure 4.32	Optical properties of 4 samples prepared at different withdrawal rates, (a) 0.1, (b) 1.0, (c) 2.0, and (d) 3.0 cm/min	126
Figure 4.33	I-V characteristics of CuO films as a function of withdrawal rates, (a) 0.1, (b) 1.0, (c) 2.0, and (d) 3.0 cm/min	127
Figure 4.34	FESEM images of CuO films deposited on (a) Al ₂ O ₃ glass and (b) ITO glass substrate	129
Figure 4.35	FESEM images of CuO films deposited on ITO glass substrate with using (a) CTAB and (b) Triton as surfactants	130
Figure 4.36	FESEM images of CuO films deposited on Al ₂ O ₃ glass with using CTAB as surfactants	131

Figure 4.37	XRD patterns of samples prepared at different annealing temperatures in air at (a) 250, (b) 300, (c) 350, (d) 400, and (e) 500 °C	133
Figure 4.38	XRD patterns of samples prepared at different annealing temperatures in Ar-H ₂ gas at (a) 250, (b) 300, (c) 350, (d) 400, and (e) 500 °C for 1 hour	133
Figure 4.39	XRD patterns for samples prepared at different annealing time at 500 °C in Ar-H ₂ gas at (a) 4 Hour and (b) 7 Hour	135
Figure 4.40	The FESEM images of samples made at different annealing temperatures: (a) 250 °C, (b) 300 °C, (c) 350 °C, (d) 400 °C, and (e) 500 °C in air.	136
Figure 4.41	I-V characteristics of CuO films prepared at different annealing temperatures: (a) 250 °C, (b) 300 °C, (c) 350 °C, (d) 400 °C, and (e) 500 °C in air.	139
Figure 4.42	XRD patterns for films prepared with optimum condition deposited on (a) glass substrate and (b) n-type ITO glass substrate	141
Figure 4.43	FESEM images of CuO films deposited on (a) glass substrate and (b) n-type ITO glass substrate made under optimum condition: 120 mmol of Cu (NO ₃) ₂ , 3 coatings, 2.0 cm/min of withdrawal rate and annealed at 500 °C for 1 hour in air.	142
Figure 4.44	AFM topography in 2-D and 3-D images of CuO films deposited on (a) glass substrate and (b) n-type ITO glass substrate made under optimum condition at 180 mmol of Cu (NO ₃) ₂ , 5 coatings, 2.0 cm/min of withdrawal rate and annealed at 500 °C for 1 hour in air.	143
Figure 4.45	Optical properties of the optimum CuO films deposited on (a) glass and (b) n-type ITO glass substrate	144
Figure 4.46	I-V characteristics of CuO/ITO p-n heterojunctions	145

LIST OF ABBREVIATIONS

TCO	Transparent Conducting Oxide
LCD	Liquid Crystal Display
OLED	Organic Light Emitting Diode
ITO	Indium Doped Tin Oxide (In: SnO ₂)
CSD	Chemical Solution Deposition
VB	Valence Band
CB	Conduction Band
CBM	Conduction Band Minimum
VBM	Valence Band Maximum
CMVB	Chemical Modulation of The Valence Band
MOD	Metal Organic Decomposition
XRD	X-Ray Diffractometer
FTIR	Fourier Transformation Infra Red
UV-VIS	Ultra Violet- Visible
AFM	Atomic Force Microscopy
FESEM	Field Emission Scanning Electron Microscope
SPA	Scanning Probe Analysis
CAO	Copper Aluminum Oxide
SMMRE	School of Materials and Mineral Resources Engineering
ICDD	International Centre of Diffraction Data
UV-VIS	Ultraviolet-Visible Spectroscopy
TG	Thermogravimetric
DTA	Differential Thermal Analysis
FWHM	Full Width Half Maximum

SCL	Space Charge Limited
SCO	Strontium Copper Oxide (SrCu_2O_2)
CTAB	Cetil Trimethyl Ammonium Bromide
TX100	Triton X100
PEG	Poly Ethylene Glycole
RMS	Root Mean Square
2-D	Two Dimension
3-D	Three Dimension

LIST OF SYMBOLS

σ	Driving Conductivity
N	Density Of Charge Carriers
μ	Carrier Mobility
E	The Electronic Charge (1.602×10^{-19} C)
E_g	Energy Gap
ρ	Resistivity
M	Molecular Weight
η	Viscosity
ϵ	Dielectric Constant
μ	Dipole Moment
λ	Wavelength of X-Ray Beam
2θ	Angle of Diffraction
D	Distance between each set of atomic planes of the crystal lattice
T	Transmittance
α	The Absorption Coefficient
$h\nu$	Photon Energy,
k	The Spring Constant
x	The Cantilever Deflection
L	The length of a side of the square
W	The thickness of the film
R	Resistance
M	Geometrical Slopes

SINTESIS DAN PENGOPTIMAAAN TERHADAP KUPRUM OKSIDA SEBAGAI OKSIDA PENGALIR LUTSINAR JENIS-P

ABSTRAK

Penyelidikan ini memberi tumpuan kepada sintesis dan pengoptimaan terhadap ciri-ciri filem nipis kuprum oksida (CuO) nipis sebagai oksida pengalir lutsinar jenis-p yang dihasilkan melalui kaedah pemendapan larutan kimia, berasaskan proses nitrat dengan menggunakan kaedah salut celup. Untuk mendapatkan keadaan terbaik pembentukan filem CuO nipis, pelbagai parameter telah dikaji termasuklah pelbagai kepekatan larutan prapenanda berasaskan kuprum nitrat, bilangan celupan, kadar pengunduran dan pelbagai jenis substrat telah digunakan. Kesan suhu penyepuhlandapan dalam keadaan dan masa yang berbeza juga dijalankan. Hasil kajian menunjukkan, fasa tunggal CuO terbentuk setelah larutan berasaskan Cu yang disalut di atas substrat kaca disepuhlandap selama 1 jam di dalam udara pada suhu 500 °C. Keadaan terbaik penghasilan filem CuO nipis yang homogen dengan kualiti salutan terbaik diperolehi. Larutan prapenanda yang digunakan haruslah mengandungi 120 mmol Cu (NO₃)₂.2¹/₂ H₂O dan dicelupkan sebanyak 3 kali dengan menggunakan kadar pengunduran sebanyak 15 cm/min. Setelah mengambil kira kesemua parameter yang dikaji, skema pembentukan filem nipis yang dicelup di atas substrat dibentangkan di dalam penyelidikan ini. Di bawah keadaan yang terbaik, ketebalan filem CuO nipis sebanyak 240 nm dengan purata agihan saiz bijian sebesar 80 nm dihasilkan. Ciri-ciri optic filem CuO nipis telah dikaji. Filem CuO nipis yang terbaik dihasilkan mempunyai kelutsinaran sebanyak 70 % didalam julat cahaya Nampak daripada 400 nm hingga 800 nm dengan jalur tenaga optik, E_g ialah 2.1 eV.

Nilai terbesar keberaliran elektrik yang dikira adalah sebanyak $2.34 \times 10^{-4} (\Omega\text{cm})^{-1}$. Setelah keadaan terbaik untuk pembentukan filem CuO nipis telah berjaya diperolehi, filem CuO nipis ini disalut di atas substrat jenis-n iaitu kaca ITO, untuk mengkaji cirri-ciri simpang p-n. Nilai keruntuhan voltan sebanyak 3 V telah diperolehi melalui kaedah penduga dua titik.

SYNTHESIS AND OPTIMIZATION OF COPPER OXIDE AS P-TYPE TRANSPARENT CONDUCTING OXIDE

ABSTRACT

The main focus of this research is to synthesis and to optimize the properties of thin copper oxides (CuO) films as a p-type transparent conducting oxide (TCO) produced by chemical solution deposition (CSD) technique through nitrate route using dip coating process. To obtain the optimum condition for the formation of thin CuO films, various parameters were studied including different concentrations, number of coatings, withdrawal rates, surfactants and different substrates were used for depositing thin CuO film. Effect of annealing temperature at different atmosphere and different annealing time were also conducted. The results showed that, single phase of CuO was formed after Cu precursor solution coated on glass substrate was annealed for 1 hour in air at 500 °C. The optimum condition for the formation of homogeneous thin CuO films with the best coating quality was identified. The precursor solution has to have concentration of 120 mmol of $\text{Cu}(\text{NO}_3)_2 \cdot 2\frac{1}{2}\text{H}_2\text{O}$ and deposition was to be done 3 times and with the use of withdrawal rate of 15 cm/min. The scheme of formation was proposed in this work after considering all of the parameters. Under this optimized condition, 240 nm thick films with an average grain size of 80 nm were produced. The optical properties of thin CuO films were studied. The optimum film has transparency of 70% from 400 to 800 nm of visible light with optical band gap value, E_g equal to 2.1 eV were obtained. The highest electrical conductivity measured was approximately $2.34 \times 10^{-4} (\Omega\text{cm})^{-1}$. After the optimum condition of the formation thin p-type CuO film successfully formed, the

film was deposited on n-ITO glass for p-n junction characterization. The diode property with 3 V of breakdown voltage was gathered by two-point probe technique.

CHAPTER 1

INTRODUCTION

1.1 Introduction

The rapid development in the field of transparent conducting oxides (TCO) as transparent conductive electrodes for many advanced technological applications such as for solar cells, flat panel displays, liquid crystal displays (LCDs) and organic light emitting diodes (OLEDs), has stimulate intensive research efforts to understand comprehensively the physical properties of this unique class of material [Ginley et al., 2000]. The unique properties of TCO that contributed to the intense investigation are the optical transparency in visible portion of light spectrum and the controllability of electronic conduction. An n-type TCO such as ZnO, SnO₂ and In: SnO₂ (ITO) has been used as electrode in various electronic and optoelectronic devices. Little has been done on the formation of active devices from this material due to the lack of p-type oxides.

The development of p-type TCO will enable the formation of transparent p-n junction based devices such as transparent diodes, transistors and light emitting diodes. Copper oxide (CuO and Cu₂O), CuAlO₂, and CuGaO₂ are examples of transparent p-type semiconductors [Kawazoe et al., 1997]. These materials are of interest because of their potential use in many technological fields which could lead to the formation of transparent electronics. The properties of the copper oxide-based semiconductors depend greatly on their composition, homogeneity and

microstructure. These three characteristics are of utmost importance and will change depending on the processing and synthesis route [Roy et al., 1996].

This thesis is focus of CuO as p-type TCO. Review articles on the synthesis process of CuO have been extensively reported such as dc-reactive sputtering, electrodeposition, reactive evaporation, thermal oxidation, anodic oxidation and sol-gel processes [Lu et al., 2009; Mahalingam et al., 2006; Balamurugan et al., 2001; Ray et al., 2001 and Musa et al., 1998]. In this work, the chemical solution deposition (CSD) process through nitrate route was selected. CSD process has the potential advantage of achieving homogeneous mixing of the component cations on atomic scale, low deposition temperatures, which together result in low cost process with inexpensive equipments, and also forming films which are of great technological importance [Schwartz et al., 2004].

The synthesis and optimization of thin CuO film was first be conducted. After the optimum condition of film deposition successfully formed, these conditions were used for deposition of p-type CuO film on the n-type ITO glass to form the transparent p-n junction devices. The simple architecture of transparent p-n junction based on CuO is shown in Figure 1.1. The applications of CuO on ITO architecture could be in the field of optoelectronics or cell-transparent transistor used mainly in display devices. CuO were selected because it is non toxic, relatively cheap and abundantly available. The main characterization studies include the structural, morphological, optical and electrical properties.

The initial content of this dissertation will have the details of review regarding the relevant concepts and literatures related to the TCO for the transparent electronic device applications. This is followed by an outline of the experimental procedures used to achieve the research objectives and discussion on the results obtained. Finally, the conclusion of this research is presented. Some suggestions and recommendation for future research activities are also given in this thesis.

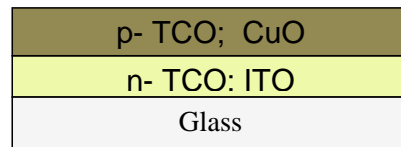


Figure 1.1 A schematic illustration of the p-n junction conducting oxide films

1.2 Problem Statement

Although the TCOs have a wide range of applications, very little work has been done on the fabrication of p-n junction active device using TCO. This is because most of the TCO are of the n-type and the corresponding p-type TCOs are not systematically investigated. Since the development of p-type TCO is one of the key component for transparent p-n junction-based devices, the formation of p-type TCO based on copper oxide is the main objective in this work. In the literature, most of the techniques used for the formation of TCO film are based on physical method and hence they are expensive and difficult to conduct compared to CSD technique which is simpler with potential for the large scale preparation of thin semiconductor films.

1.3 Objectives

- i. To determine an optimum condition for the formation of thin p-type copper oxide film by chemical solution deposition (CSD) technique.
- ii. To study the properties of the thin copper oxide films based on structural, morphological and optical characteristics.
- iii. To investigate the electrical properties of the thin copper oxide film
- iv. To form a p-n junction by depositing thin p-type copper oxide film on n-type ITO coated on glass and to characterize its properties.

1.4 Expected Outcomes

- i. The thin CuO films are formed by chemical solution deposition (CSD) technique.
- ii. Deposition mechanisms of thin CuO films are proposed to understand the deposition process better and to explain the CSD process.
- iii. The preparation of p-n junction based on p-type TCO of copper oxide deposited on ITO glass.

CHAPTER 2

LITERATURE REVIEW

2.1 Introduction

In this chapter, the overview of transparent conducting oxide (TCO) will be discussed. The discussion will begin with the topic related to the TCO, methods of formation of the TCO film and also relevant previous works on TCO. As this dissertation is mostly concerned on the formation of thin copper oxide film as a p-type TCO, thus the material will be focused and discussed. Further, the formation of transparent p-n junction through the deposition of p-type TCO on n-type TCO will also be reviewed.

2.2 Transparent Conducting Oxides (TCO) Thin Film

Transparent conducting oxide (TCO) consists of a group of materials that shows simultaneously high transparency of visible light ($> 80\%$) and high electrical conductivity ($> 10^3$ S/cm) [Lewis et al., 2000]. It is known that, there are three groups of materials classified based on the electrical properties; metal, semiconductor and insulator. Metals are highly conductive with small band gap values and are not transparent. Highly transparent materials have high band gap value but they are insulators. TCO semiconductors on the other hand, are transparent and electrically conductive. TCOs have band gap values ranging from 2.0 to 4.0 eV [Fan et al., 1977]. These make TCOs not only transparent but at the same time

conductive. These unique properties of TCOs have made them very attractive for applications in optoelectronics and as electrode in flat panel displays.

Figure 2.1 shows the band gap structure for TCO. Generally, visible light in range from 2.1 to 3.1 eV does not have enough energy to excite electrons from valence band (VB) to conduction band (CB) band edge, but has enough energy to excite holes (free carrier for p-type) from acceptor level to VB or electrons (free carrier for n-type) from donor to CB. These acceptor and donor levels can be produced in TCO material either by introducing non-stoichiometry and (or) using appropriate dopants within the materials [Exarhos et al., 2007].

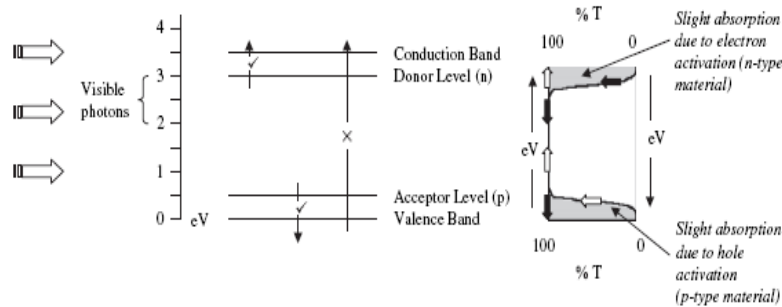


Figure 2.1 Schematic illustrating the band gap designing for TCO [Chattopadhyay et al., 2005]

From Figure 2.1, on the right hand side, the optical properties of TCO materials were shown. The white arrow (\Leftrightarrow) indicates the transmittance graph for p-type TCO, in which slight absorption can be observed as indicated by shaded area due to the activation of holes from acceptor level to VB at lower energy. The black arrow (\blackrightarrow), on the other hand, indicates the transmittance graph for n-type TCO,

with slight absorption occurred due to the activation of electrons from donor level to CB at lower energy [Chattopadhyay et al., 2005].

2.3 Thin Films

2.3.1 Advantages compared with traditional bulk materials

The basic properties of thin film, such as film composition, crystal phase and orientation, film thickness and microstructure, are controlled by the deposition conditions. Thin films exhibit unique properties that cannot be observed in the bulk materials [Riad et al., 1997]:

- Unique properties resulting from the atomic growth process
- Size effects, including quantum size effects, characterized by the thickness, crystalline orientation and multilayer aspects.

In thin films, deviations from the properties of the corresponding bulk materials arise because of their small thickness, (for example, while the structure may be macroscopically large in length and width, it may have a thickness that is only on the order of a micron or less), large surface-to-volume ratio and unique physical structure which is a direct consequence of the growth process. Thin films do not have to be planar. The properties of such thin film structures are strongly influenced by the surface properties and may be very different from that of the same material in bulk form. The thin film may consist of a pure material, or a composite or a layered structure, and several of the thin films may be present in a more complex device.

2.3.2 Thin film growth mode

The growth of thin films can be categorized into three different modes as shown in Figure 2.2, which was first introduced by Ernst Bauer in 1958 [Greene et al., 1993 and Liu et al., 1999]. Island growth (Volmer-Weber) results in the formation of isolated islands on the surface. This occurs when the cohesive energy of the atoms within the film is greater than the cohesive energy between the film and atoms on the surface.

Layer-by-layer growth (Frank-van der Merwe) involves a deposition of one monolayer at the time and results in a very smooth epitaxial film. Growth mode arises when the atoms of the deposited material are more strongly attracted to the substrate than they are to themselves. The cohesive energy will decrease as each film layer is added.

Mixed growth mode (Stranski-Krastanove) involves growth of islands after the first monolayer has been formed successfully. This occurs when the decrease in binding energy is energetically control by other factors such as strain due to lattice mismatch, with the result that island formation becomes more favorable.



Volmer - Weber mode

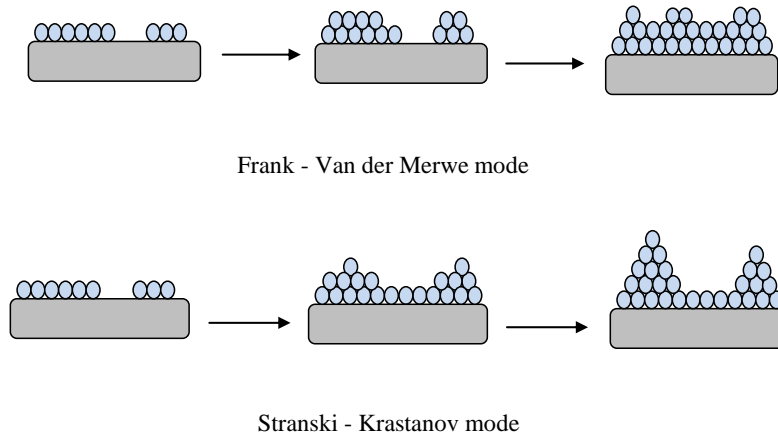
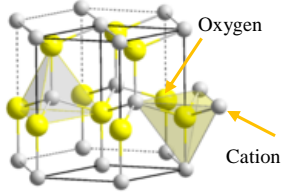
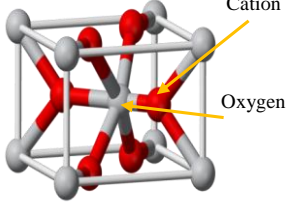
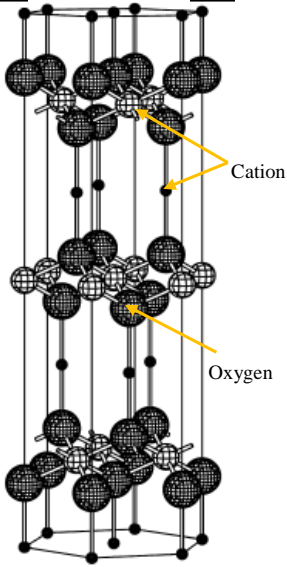


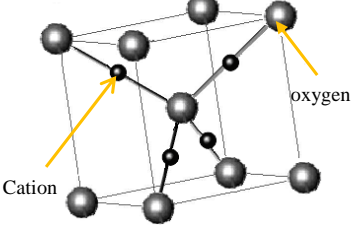
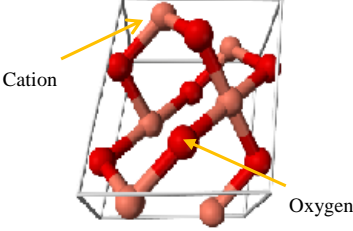
Figure 2.2 Common modes of film growth; (a) Island (Volmer - Weber) mode, (b) layer-by-layer (Frank-Van der Merwe) mode and (c) Mixed (Stranski-Krastanov) mode

2.4 Different Types of TCO Materials

TCO is a materials that has show transparency in a limited and well-defined range, normally encompassing visible light in the $0.4 < \lambda < 0.7 \mu\text{m}$ wavelength interval. In the infrared (IR) their metallic property leads to reflectance and at sufficiently short wavelength, in the ultraviolet (UV), they become absorbing due to excitations across an energy gap. There are two types of TCO, n- and p-type. The majority of TCO are n-type semiconductors such as indium tin oxide (ITO) and ZnO. A number of p-type TCO have recently developed, such as the delafossite CuAlO_2 , CuInO_2 and CuGaO_2 . Cubic and monoclinic of Cu_2O and CuO are also well known [Chattopadhyay et al., 2005]. Table 2.1 shows the crystal structures of most commonly studied p- and n-type TCO.

Table 2.1 Crystal structures of most commonly studied p- and n-type TCOs [Barsoum et al., 2003; Yanagi et al., 2000; Kawazoe et al., 1997]

Type of Crystal Structure	Illustration of the Crystal Structure	Materials and their Band Gaps
Wurtzite		n- type; ZnO $E_g \sim 3.3 \text{ eV}$
Rock salt		n- type; CdO, SnO₂, In₂O₃, CdIn₂O₄, Cd₂SnO₄ and etc. $E_g \sim 3.0 \text{ eV}$
Delafossite		p- type; CuAlO₂, CuGaO₂, SrCu₂O₂ $E_g \sim 3.5 \text{ eV}$

Cubic		<p>p-type; Cu₂O</p> <p>$E_g \sim 2.1 \text{ eV}$</p>
Monoclinic		<p>p-type; CuO</p> <p>$E_g \sim 1.5 \text{ eV}$</p>

2.4.1 n- Type TCO

To achieve n-type conductivity in a transparent metal oxide, the introduction of defect energy levels such as oxygen vacancies, impurity substitutions and interstitials that can donate electrons (free carriers for n-type conductor) to the metal oxide conduction band are required. For example, when aluminium is introduced as a dopant to zinc oxide under reducing conditions, the aluminum defect energy levels lie close to the conduction band minimum (CBM) thereby allowing promotion of free carriers into the conduction band inducing an increase in conductivity. Therefore, the suitable dopants are required to make materials exhibit a relatively high electron affinity and created defect energy levels close to the CBM [Exarhos et al., 2007]. Table 2.2 shows the electrical properties of several common n-type TCOs and their energy gap as summarized by Jia et al., (2002).

Table 2.2 The electrical properties of different n-type TCOs [Jia et al., 2002]

<i>n-type TCO Materials</i>	<i>Energy gap, E_g (eV)</i>	<i>Resistivity ($m\Omega.cm$)</i>	<i>Carrier concentration ($10^{20} cm^{-3}$)</i>	<i>Hall mobility [$cm^2/(V.S)$]</i>
ZnO	3.2	9	0.23	-
In ₂ O ₃ :Sn (ITO)	3.7	0.4	14.5	29
GaInO ₃	3.4	2.5	4	10
MgIn ₂ O ₄	3.5	0.43	6.3	22

2.4.2 p-Type TCO

As mentioned earlier, most of the TCO materials are n-type. Although n-type TCO has higher conductivity, the applications are limited to the use as transparent conductive electrode. Many active functions of semiconductor devices are based on the activity of a p-n junction. Due to the lack of p-type TCOs, not many devices are produced. The fabrication of a transparent p-n junction is the most fundamental step in realizing transparent electronics. Therefore, both p- and n-type TCOs are required to form a transparent p-n junction. It is of the utmost importance to prepare new types of p-TCOs with better optical and electrical characteristics that can be used in new applications such as transparent diode, transistor and others optoelectronic applications.

To achieve p-type conductivity in a transparent metal oxide, the introduction of defect energy levels such as hole doping by ionized cation vacancies, impurity acceptor ion substitutions and/or oxygen interstitials which act as electron acceptors from the metal oxide valence band (free carriers for p-type conductor) are required. In other words, the suitable dopants and/or non-stoichiometry produced within the p-

type TCO materials will contribute to energy level that are close to the valence band maximum (VBM). Therefore, electron promotion to these defect levels creates holes in the valence band thereby promoting conductivity.

2.4.2.1 Origin of Conductivity of p-Type TCO

Conductivity, σ of p-type TCO materials is generally related to the density of charge carriers (holes), n and the carrier mobility (holes mobility), μ (equation 2.1)

$$\sigma = n\mu e \quad (2.1)$$

where e is the electronic charge given by 1.602×10^{-19} C. According to the equation, to get high conductivity value, the hole density and hole mobility must be high. However, hole mobility is highly dependable on its scattering centre. Scattering centres are non-stoichiometry defects and impurities. In polycrystalline material, grain boundaries are scattering centres. This will reduced transmission, and increases the resistivity due to a decrease in hole mobility.

Although conductivity of p-type TCO is mostly depending by hole conduction, however, in most of the binary metal oxide, the material has strong localization of holes at oxygen 2p levels. The O 2p level is far lower than the valence orbit of the metal atoms, therefore a deep acceptor level by holes formed. Hence holes require high energy to overcome a large barrier height in order to migrate within the crystal lattice, resulting in poor conductivity and hole mobility [Chattopadhyay et al., 2005].

An approach to resolve this problem is to introduce a degree of covalency on metal-oxygen bondings. Here, the valence band edge should be modified by mixing orbitals of appropriate counter cations that have energy-filled-levels comparable to the O 2p level thus the delocalization of holes occurred due to loss of strong columbic force by oxygen ions. This is the essential approach to obtain p-type TCO, which is called Chemical Modulation of the Valence band (CMVB) [Yanagi et al., 2000] as schematically shown in Figure 2.3.

Besides, there are some structural requirements for designing p-TCO materials. The important part is that the VB maximum should have low effective mass to give shallow acceptor levels (where an increase of delocalization of holes at the VB edge occurred). The more usual case is closed shell p^6 system. The problem is that the O 2p states tend to form non-bonding levels at the top of the VB. Non-bonding states always have a high effective mass, and so they give deep hole levels.

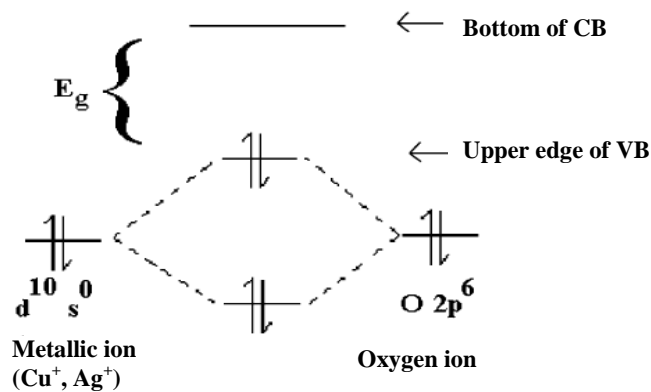


Figure 2.3 Schematic diagram of modulation of band structure (CMVB). Cations are assumed to have a closed shell the energy of which is equivalent to that of O 2p⁶. [Chattopadhyay et al., 2005]

A way to resolve this problem is to use a cation with closed shell levels, which are degenerate with the O 2p states. Cu and Ag have the appropriate d^{10} states for this purpose. The metals states interact with some of the O 2p states, which push up a more dispersive band above the non-bonding O 2p or Cu 3d states. This band has a lower effective mass producing a shallow acceptor level [Kawazoe et al., 2000].

In this regard, Cu_2O is an intrinsic p-type semiconductor, which follows this idea. However, its band gap of only 2.1 eV is too small. This is probably due to the three dimensional interactions between $3d^{10}$ electrons of neighboring Cu^+ ions (Cu-Cu coordination). The repulsive interactions occurred between the Cu^+ ions expand the band width and reduce the band gap energy. Therefore, a reduction of these repulsive interactions might be favorable for enlarging band gap for transmitting visible light. This occurs in CuAlO_2 where the O-Cu-O form separate units and the Cu-Cu coordination is reduced thus increasing the band gap and particularly decreasing the conduction band width. Since Cu_2O and CuO have the similar electronic structure with CuAlO_2 , the review of CuAlO_2 delafossite crystal structure was used to understand more on Cu-O based materials.

2.4.2.2 Delafossite Crystal Structure

One popular group of p-TCO is materials with delafossite crystal structure, such as CuAlO_2 , CuGaO_2 and SrCu_2O_2 . Materials with delafossite crystal structure (Figure 2.4) has chemical formula of $\text{A}^{\text{I}}\text{B}^{\text{III}}\text{O}_2$, where A^{I} is monovalent ions (Cu^+ , Ag^+) and B^{III} is a trivalent cations (Al^{+3} , Ga^{+3} , In^{+3} and etc). This group of materials

has attracted alternative stacking of A^I and layers of nominal $B^{III}O_2$ composition consisting of $B^{III}O_6$ octahedral sharing edges. Each A^I atom is linearly coordinated with two oxygen atoms to form an O- A^I -O dumbbell unit placed parallel to the c-axis. O-atoms of O- A^I -O dumbbell link all A^I layers with the $B^{III}O_2$ layers. On the other hand each oxide ion in the $B^{III}O_2$ layer forms a pseudo-tetrahedral coordination ($B^{III}A^I O$) [Yanagi et al., 2000] with the neighboring B^{III} and A^I ions.

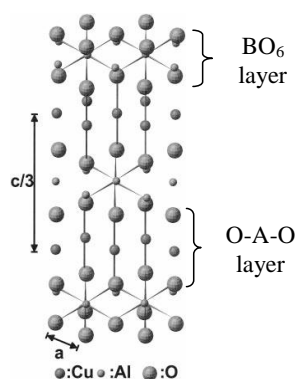


Figure 2.4 Crystal structure of delafossite consisting of stacked layers of -O-Ga(Al)-O-Cu-O- in this order along the c-axis [Yanagi et al., 2000].

Hence, as previously mentioned this electronic configuration reduces the non-bonding nature of the oxide ions and therefore delocalizes the holes at the valence band edge. Secondly, this dumbbell layered structure effectively reduces the dimension of cross linking of A^I ions thus enlarging the band gap [Kawazoe et al., 1997]. Finally, another important factor in this structure is the low coordination number of the A^I ions, due to the large separation from oxygen ligands, which is the result of the strong columbic repulsion between 2p electrons in oxygen ligands and $A^I d^{10}$ electrons. This leads to the $A^I d^{10}$ energy levels almost comparable to the O 2p

level, resulting in a high degree of mixing of these levels. Table 2.3 shows the electrical properties of different p-type TCOs.

Table 2.3 The electrical properties of different p-type TCOs [Jia et al., 2002; Nair et al., 1999; Kose et al., 2008]

<i>p-type TCO Materials</i>	<i>Energy gap, E_g (eV)</i>	<i>Resistivity ($m\Omega.cm$)</i>	<i>Carrier concentration ($10^{20} cm^{-3}$)</i>	<i>Hall mobility [$cm^2/(V.S)$]</i>
CuAlO₂	3.5	1052	0.0013	10.4
CuGaO₂	3.6	15873	0.017	0.23
SrCu₂O₂	3.3	20704	0.0061	0.46
CuO	1.9	142857	-	-
Cu₂O	2.1	228832	-	-

2.5 Applications of TCO Thin Film

Transparent conductive oxides (TCO) have been widely used as transparent conductive electrodes for solar cells and flat panel displays including liquid crystal display (LCD) and organic light emitting diode (OLED) because of their unique properties of optical transparency in visible region and controllability of electrical conductivity. The development of p-TCO has led to the new improvement in optoelectronic application such as flat panel display, transparent diode and transistor and also heterojunction in solar cell [Minami et al., 2005].

2.5.1 Flat Panel Display

Flat panel displays are commonly electronic components that have developed the way that fixed and variable information can be displayed to single or multiple viewers. They dominate many aspects of our daily lives, at home and at work, and have facilitated many new applications- particularly in the fields of hand-held and portable equipment. Indeed, mobile phones, calculators, laptop computers, portable projectors and a wide variety of other equipment and instruments could not exist without flat panel displays. The manufacturing of flat panel displays is a dynamic and continuously developing industry. Improvements in flat panel displays are made rapidly as technology improves and new discoveries are made by display scientists and engineers.

2.5.2 Functional Window

The discovery of p-type TCO has led to the fabrication of transparent electronic. For example, the combination of two types of TCO which is p- and n-type TCO (formation of p-n junction) were fabricated to produce functional windows. Functional windows are used to absorb the UV-radiation from sun's radiation to produce electric energy. Besides, it can be a good thermal electronic material.

2.6 Copper Oxide Thin Film

There are two well known copper oxides: Cu_2^+O (cuprite) and Cu^{2+}O (tenorite) [Oral et al., 2004]. Cu_2O has a cubic crystal structure with energy gap

value 2.1 eV and CuO has a monoclinic crystal structure with energy gap value 1.9 eV [Ray et al., 2001]. An important advantage of using copper oxide in device application is that it is low cost, non-toxic, and its constituents are available in abundance.

2.6.1 Cuprous Oxide (Cu₂O)

Cuprous oxide (Cu₂O) is a semiconductor, with a varying electrical and optical behavior because of the stoichiometric deviation arising from its preparation methods. Because of the advantage of high optical absorption coefficient combined with nontoxicity and low cost productivity, Cu₂O films find diverse field of applications such as oxygen and humidity sensors, electrochromic devices and absorber layer in heterojunction thin film solar cells. Scientific investigations on Cu₂O thin films have been carried out by many authors since Cu₂O is an excellent candidate for p-type TCOs. Table 2.4 shows a compilation of basic physical parameters for Cu₂O.

2.6.2 Cupric oxide (CuO)

Copper (I) oxide or cupric oxide (CuO, *tenorite*) is also a p-type transparent conducting oxide with band gap of 1.9 eV. The properties of CuO are summarized in Table 2.4. CuO has been employed as heterogeneous catalysis and gas sensor. Since the oxide is transparent in the visible part of the solar spectrum, CuO has also been used in photovoltaic applications and in photoelectrochemical cell. The ongoing interest in the fabrication of CuO films for these applications is inspired mostly by

the non-toxicity of the material, its abundance in nature and the possibility of a production of high quality films at low temperature using non-physical based method thus suitable for large scale industrial production.

Table 2.4 Physical Properties of Cu₂O and CuO

<i>Property</i>	<i>Cu₂O</i> [Mahalingam et al., 2006]	<i>CuO</i> [Alkoy et al., 2005]
Crystal structure	Cubic	Monoclinic
Band gap	2.1 eV	1.9 eV
Activation energy	0.85 eV	0.15 eV
Conductivity (as made)	$\sim 10^{-6} (\Omega\text{cm})^{-1}$	$\sim 10^{-3} (\Omega\text{cm})^{-1}$
Conductivity (as annealed at 350°C)	$\sim 10^{-3} (\Omega\text{cm})^{-1}$	$\sim 10^{-1} (\Omega\text{cm})^{-1}$
Optical transparency	Transmit at $\lambda < 1000\text{nm}$ (80%)	Transmit at $\lambda < 800\text{nm}$ (80%)
Semiconducting property	p-type	p-type
E-k	Direct	Direct

2.7 Deposition Techniques for Copper Oxide Thin Films

The actual technique for growth of thin films plays the most significant role in determining the properties of the films. Different deposition method yield films with different structural, optical and electrical properties. Even for the same deposition method, a slight variation in the deposition parameters produces films with different properties. Thus, it is very important to study the properties of various films produced by different deposition routes. In this section will discuss the nature of several types of deposition techniques, just for comparison.

Ever since Kawazoe et al., (1997) reported the synthesis of transparent p-type semiconducting thin films, various groups around the world have reported on the p-type TCO for fabrication of p-n junction transparent diodes with considerably good electro-optical properties for potential applications in transparent electronics [Banerjee et al., 2007]. Especially by using Cu-O based materials as a p- TCO. Table 2.5 represents a list of the research works on thin p-type TCOs films based on Cu-O using different deposition techniques from 1996 to 2009.

Table 2.5 List of the research works on thin p-type TCOs films based on Cu-O using different technique of deposition

Research Group	Year	p-type TCOs	Deposition Technique
Lu et al.	2009	Cu ₂ O and CuO	Reactive Magnetron Sputtering
Elangovan et al.	2008	CuO and Cu ₂ O	Thermal oxidation
Rhee et al.	2008	Cu ₂ O	Reactive Magnetron Sputtering
Kose et al.	2008	Cu ₂ O and CuO	Chemical Solution Deposition
Shishiyanu et al.	2008	Cu ₂ O	Chemical Bath Deposition
Mahalingam et al.	2006	Cu ₂ O	Electrodeposition
Sheng et al.	2006	Ca-doped SrCu ₂ O ₂	Pulsed Laser Deposition
Papadimitropoulos	2006	CuO and Cu ₂ O	Thermal oxidation
Akimoto et al.	2006	Ni-doped Cu ₂ O	Reactive Magnetron Sputtering
Reddy et al.	2005	Cu ₂ O	Reactive Magnetron Sputtering

Alkoy et al.	2005	CuO, Cu ₂ O and CuAlO ₂	Pulsed Magnetron Sputtering
Necmi et al.	2005	CuO and Cu ₂ O	Chemical Deposition
Morales et al.	2005	CuO	Spray-Pyrolisis
Oral et al.	2004	CuO	Sol-gel Technique
Lidia et al.	2003	CuO and Cu ₂ O	Sol-gel technique
Pierson et al.	2003	Cu ₂ O and CuO	Reactive Sputtering
Kazuhiko et al.	2002	CuAlO ₂	Solution Method
Georgieva et al.	2002	Cu ₂ O	Electrodeposition
Ray et al.	2001	Cu ₂ O and CuO	Sol-gel technique
Balamurugan et al.	2001	Cu ₂ O	Activated Reactive Evaporation
Ghosh et al.	2000	Cu ₂ O and CuO	Reactive Sputtering
Nair et al.	1999	Cu ₂ O and CuO	Chemical Deposition
Musa et al.	1998	Cu ₂ O	Thermal Oxidation
Kawazoe et al.	1997	CuAlO ₂	Reactive Sputtering
Golden et al.	1996	Cu ₂ O	Electrochemical Deposition

2.7.1 Sputtering

Lu et al. (2009) had prepared copper oxide thin film by using dc-reactive magnetron sputtering of pure copper target in a mixture of argon and oxygen gases. They found that, oxygen partial pressure is a crucial parameter in controlling the phases and the physical properties of the deposited copper oxide thin films. Single-phase Cu₂O thin films with cubic structure were obtained at low oxygen partial pressure between 0.147 Pa and 0.200 Pa while higher oxygen partial pressure

promoted the formation of CuO thin films with base-centered monoclinic structure. Polycrystalline Cu₂O thin films deposited with oxygen partial pressure at 0.147 Pa possessed the lowest p-type resistivity of 1.76 Ω cm as well as an optical band gap of 2.01 eV. On the other hand, polycrystalline CuO thin films deposited with oxygen partial pressure at 0.320 Pa were also single phase but showed an n-type resistivity of 0.19 Ω cm along with an optical band gap of 1.58 eV.

2.7.2 Thermal Oxidation

Thermal oxidation technique has been done by Elangovan et al., (2008). In this process, a thin film of Cu is first deposited by e-beam evaporating of the Cu pellets on a substrate. The thermal oxidation of Cu is then carried out in air at annealing temperature from 100 to 450°C for 30 min. It is demonstrated that the cubic Cu phase of the as-deposited films changes into single cubic Cu₂O phase for the annealing between 200 and 300°C and whereas the films annealed between 350 and 450°C show a single monoclinic CuO phase. According to their results, they reported that the films with dominating Cu₂O phase are p-type conducting, however, a relatively poor crystallinity of these films limited the p-type characteristics. The post-annealing is found to be effective on the distribution of grains and their sizes. The transmittance value was increased to a maximum 80% on annealing at 200°C with the direct band gap varied between 2.03 and 3.02 eV.

2.7.3 Electrodeposition

Electrodeposition Cu_2O thin films has been reported by several researchers. These include Georgieva et al., (2002), Tang et al., (2005) and Mahalingam et al., (2006). In this process, a simple apparatus was used. It consisted of a thermostat, a glass with a solution, two electrodes (cathode and anode) and a standard electrical circuit for electrolysis. Here, platinum and saturated calomel electrode is commonly used as counter electrode and reference electrodes, respectively. Georgieva et al. reported that, polycrystalline Cu_2O films of 4-6 μm thickness were obtained with 2.38 eV optical band gaps which offer wider possibilities for application both in metal-semiconductor and heterojunction cells configuration. Tang et al., (2005) on the other hand, reported that the Cu_2O thin film was formed at 300°C and the electrical resistivity decreases as annealing temperature increases with the optical band gap is 2.06 eV. Mahalingam et al., (2006) also showed the same result. The Cu_2O phase was transformed to CuO when further oxidation occurred with increased annealing temperature.

Therefore, in regards to sputtering, thermal oxidation and electrodeposition, although a quality thin film can be formed using all these three favorable methods, many things need to be considered. These include target composition, sputtering power, substrate temperature during deposition, oxygen partial pressure and residual water-vapor partial pressure. However it is very complicated process and only a small area deposition can be done. Therefore, a new technique needs to be used which is easier, inexpensive and has a large area deposition. The most suitable

technique that follows this requirement is chemical solution deposition (CSD) technique.

2.7.4 Chemical Solution Deposition (CSD) Methods

The general principal involved in CSD is the preparation of a homogeneous precursor solution containing metallic cations. The precursors are dissolved in appropriate solvents and mixed to yield the desired composition of the final film. The next processing step is the deposition of the coating solution on the substrate either by spin coating using a rotating substrate, spray coating the misted solution or dip coating in a solution bath. After coating, the substrate is dried at low temperature and dipped again to produce multiple coatings. Finally, the as-deposited film is through an annealing process. During drying, the decomposition of the organic matrix in air or oxygen occurs and during the annealing process, crystallization and densification of the films occurs.

CSD can be grouped into different groups like sol-gel, metal-organic decomposition, pechini or nitrate route, which depends on the precursor solution used, gelation behavior of the deposited solution and the reaction that occurs during annealing. For the formation of CuO by CSD, it appears that only a few works are available in literature [Ray et al., 2001]. As this method has not been fully explored, there is a wide area that can be studied. Compared with other processes, CSD methods present several advantages such as: low temperature processing, arbitrary substrate shapes, controllable film thickness and morphology and potentially low-cost [Ray et al., 2001]. Figure 2.5 shows the CSD method. From the figure, the grey